



Published in final edited form as:

Nat Chem. 2018 March ; 10(3): 251–258. doi:10.1038/nchem.2917.

Engineered modular biomaterial logic gates for environmentally triggered therapeutic delivery

Barry A. Badeau¹, Michael P. Comerford¹, Christopher K. Arakawa², Jared A. Shadish¹, and Cole A. DeForest^{1,2,3,4,*}

¹Department of Chemical Engineering, University of Washington, Seattle, WA 98105, USA

²Department of Bioengineering, University of Washington, Seattle, WA 98105, USA

³Institute of Stem Cell & Regenerative Medicine, University of Washington, Seattle, WA 98109, USA

⁴Molecular Engineering & Sciences Institute, University of Washington, Seattle, WA 98105, USA

Abstract

The successful transport of drug- and cell-based therapeutics to diseased sites represents a major barrier in the development of clinical therapies. Targeted delivery can be mediated through degradable biomaterial vehicles that utilize disease biomarkers to trigger payload release. Here, we report a modular chemical framework for imparting hydrogels with precise degradative responsiveness by using multiple environmental cues to trigger reactions that operate user-programmable Boolean logic. By specifying the molecular architecture and connectivity of orthogonal stimuli-labile moieties within material crosslinkers, we show selective control over gel dissolution and therapeutic delivery. To illustrate the versatility of this methodology, we synthesized seventeen distinct stimuli-responsive materials that collectively yielded all possible YES/OR/AND logical outputs from input combinations involving enzyme, reductant, and light. Using these hydrogels we demonstrate the first sequential and environmentally stimulated release of multiple cell lines in well-defined combinations from a material. We expect these platforms will find utility in several diverse fields including drug delivery, diagnostics, and regenerative medicine.

Graphical Abstract

Users may view, print, copy, and download text and data-mine the content in such documents, for the purposes of academic research, subject always to the full Conditions of use: http://www.nature.com/authors/editorial_policies/license.html#terms

*Correspondence to: profcole@uw.edu.

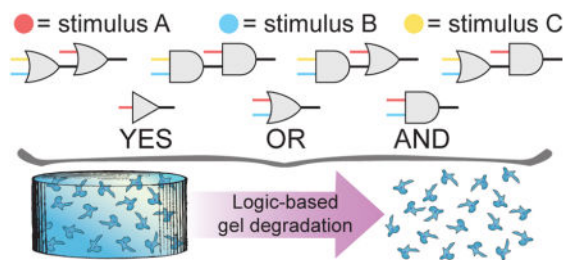
Data availability: The characterization data and experimental protocols for this work are available within this manuscript and its associated Supplementary Information, or from the corresponding author upon request.

Author contributions:

For this manuscript, B.A.B. and C.A.D. conceived and designed the experiments; B.A.B., M.P.C., C.K.A., and J.A.S. performed the experiments; B.A.B. and C.A.D. analyzed the data and prepared the figures; B.A.B. and C.A.D. wrote the paper.

Competing financial interests:

The authors declare no competing financial interests.



Main text

Recent innovations in therapeutic development and cell engineering have yielded powerful tools to combat an increasing number of debilitating and life-threatening diseases. Despite these advances, several barriers to clinical translation remain, including the significant challenge of limiting therapeutic deployment to sites of disease that can be widespread and unknown^{1–4}. Targeted delivery strategies that exploit disease-related biomarkers improve treatment efficiency and efficacy by reducing dosage requirements and adverse off-target effects^{4–8}. Most typically, these methods employ polymer-based vehicles to facilitate delivery and protect therapeutic cargo from immune recognition, clearance, and non-specific cellular uptake. Cell-based therapies further necessitate that these vehicles recapitulate critical aspects of native tissue to ensure sustained cell viability and function. Hydrogels offer promise in each of these regards, as they are robust material platforms whose biochemical and biophysical properties can be tuned to preserve and promote specific cell fates, are readily formulated into a variety of shapes and stiffnesses to control transport to and within tissues, and can be engineered to degrade in response to locally presented cues to facilitate therapeutic release^{9,10}.

Smart materials have been engineered to leverage pathophysiology for targeted delivery by integrating functional groups that cleave or change conformation in response to an external stimulus (e.g., enzyme, pH, temperature, redox conditions, small molecules), allowing them to sense and respond to disease-associated biochemical hallmarks^{3,4,7}. Though materials sensitive to single factors can enrich therapeutic delivery to sites of disease, individual biomarkers are rarely unique to these locations, leading to suboptimal selectivity. For example, cancer microenvironments have been targeted through their extensive matrix metalloproteinase (MMP) activity, reducing conditions, and subphysiological pH; however, these characteristics are respectively shared by healthy joints¹¹, the intracellular milieu⁴, and the stomach. To improve site-specificity of payload release, materials that degrade only when presented with multiple cues have been developed^{3,12–19}. While previous approaches have enabled therapeutic delivery in response to two environmental factors, they lack a generalizable framework to exploit additional input stimuli to further refine release specificity. Moreover, the uniqueness of each previously reported responsive platform necessitates a complete material redesign – one that is generally not synthetically tractable due to inherent constraints on material composition and vehicle geometry – in order to alter the response profiles or utilize different biochemical triggers. Further, the subset of

degradable materials demonstrated for live cell release has been limited to single biological inputs^{20–23}, confining next-generation cellular therapeutics to simple delivery platforms.

To address these technological limitations and enable unprecedented specificity over controlled therapeutic release, we sought to develop a versatile chemistry-based approach to create multi-stimuli responsive hydrogel platforms that are (i) able to perform biocomputation, (ii) modular in design, and (iii) fully cytocompatible. Biocomputation represents the ability to simultaneously sense multiple biologically presented inputs and follow a user-programmed Boolean logic-based algorithm to provide a functional output⁷, demonstrated here in the form of material degradation and therapeutic delivery. System modularity allows both the inputs and the logical functions to be changed and combined to generate a theoretically limitless number of novel materials, each with unique and user-specified release characteristics. Furthermore, exploitation of cytocompatible bioorthogonal chemistries permits responsive material platforms to be formed and degraded on demand in the presence of live cells, representing a major improvement over existing cell delivery strategies.

In our rational design-based approach, stimuli-sensitive components are incorporated into discrete, monodisperse, synthetic crosslinkers that, upon reaction with polymer macromers, form hydrogels of well-defined molecular architecture. Information governing the environmental-responsiveness of the resulting material is embedded within the crosslinker domain; when the linker is covalently cleaved, the material degrades and simultaneously releases any encapsulated or tethered payload. The simplest Boolean logical function, the YES-gate, is implemented when a single stimuli-labile moiety is included in the linker. We hypothesized that more advanced logical operations could be built through the controlled connectivity of additional cleavable groups within a crosslinker. When two degradable units are connected in series, the cleavage of either moiety causes material dissolution, forming an OR-gate (denoted with logic symbol \vee); when two degradable units are connected in parallel, the cleavage of both moieties is required for material dissolution, forming an AND-gate (denoted by logic symbol \wedge). These concepts can be expanded hierarchically, combining multiple gates into a logical circuit to engineer complex responses to additional dynamic stimuli (Fig. 1). Formalizing the relationship between crosslinker architecture and hydrogel degradability provides a template for creating materials that are structurally simple yet functionally complex.

Results

Synthesis of logic-based responsive crosslinkers

Implementation of the outlined biocomputational strategy requires precise control over crosslinker functionality and architecture. We used peptide-based crosslinkers due to the efficiency of solid-phase peptide synthesis in generating monodisperse macromolecules that contain a range of functional groups with sequence-defined order and connectivity. Peptides, which possess intrinsic biocompatibility, can be chemically modified to introduce non-canonical functionality, connectivity (e.g., branching, cyclization, intramolecular stapling), and degradability. As a demonstration of this logic-based approach, three chemically orthogonal stimuli-labile moieties from different reaction classes were employed: (i) the

enzymatically degradable oligopeptide sequence, GPQG↓IWGQ, which cleaves in the presence of MMPs and allows for cell- and disease-triggered response²⁴; (ii) disulfide bonds, which degrade under reducing conditions present both intracellularly and in disease states; and (iii) an *ortho*-nitrobenzyl ester (*o*NB), which undergoes photocleavage upon cytochrome near-UV light exposure ($\lambda = 365$ nm), thereby facilitating user-defined spatiotemporal control over material properties²⁵ (Fig. 1E). Exhaustively spanning all hierarchical YES/OR/AND combinations of these three stimuli-labile moieties, we synthesized seventeen distinct crosslinkers that each exhibited a unique logical output (Supplementary Methods 1–21). Each crosslinker was flanked with two reactive azide moieties to enable formation of nearly ideal step-growth hydrogel networks *via* a strain-promoted, azide-alkyne cycloaddition (SPAAC) reaction²⁶ with four-arm poly(ethylene glycol) tetrabicyclononyne (PEG-tetraBCN, Supplementary Method 22). SPAAC click chemistry rapidly produces homogenous hydrogels in a bioorthogonal fashion, thereby permitting encapsulation of bioactive therapeutics and living cells^{27–29}. Moreover, an extensive toolbox of SPAAC-compatible modifications allows for uniform network functionalization with moieties ranging from small molecules to full-length proteins^{29–32}. Such tunability further enables the design of complex delivery vehicles, for example, through the inclusion of targeting moieties, instructive cues to guide encapsulated cell fate and function, or tethered therapeutics to be released upon material dissolution.

Assessing solution-based crosslinker degradation in response to environmental stimuli

To demonstrate that crosslinkers degrade as engineered in response to environmental cues and that stimuli-responsive reactions are chemically orthogonal, we treated each of the one- and two-input linkers with every possible combination of MMP enzyme (E), reducing components (R), and light (P) (Supplementary Methods 23 and 24). Reaction products were characterized using matrix-assisted laser desorption/ionization time-of-flight mass spectrometry (MALDI-TOF). Detected masses were in excellent agreement with those of the expected reaction products (Fig. 2, Supplementary Figs. 1–9), indicating that the linkers respond as designed on a molecular level. To further investigate, the enzyme AND photo linker (E \wedge P) was pretreated with different combinations of enzyme and light, added to a stoichiometrically defined amount of PEG-tetraBCN, and characterized by *in situ* oscillatory rheology to monitor evolution of material properties (Supplementary Methods 22 and 25). Untreated E \wedge P yielded robust gels, demonstrating the first successful use of a cyclic or stapled peptide for material crosslinking. Final storage moduli of samples containing the untreated linker ($G' = 1660 \pm 170$ Pa) were similar to that of the linkers subjected to either enzyme or light ($G' = 1580 \pm 130$ Pa and 1540 ± 110 Pa, respectively), while the linker treated with both enzyme and light did not form a gel ($G' = 200 \pm 30$). All samples had a final loss modulus (G'') of ~ 50 Pa. Consistent with rubber elasticity theory where shear moduli scales with crosslinking density³³ and calculations that distances between network branch points increase 3% upon cleavage of a single arm of AND-gated linkers (Supplementary Method 26), this data suggests that the mechanical properties of these materials depend only on the final logical state of the Boolean linker.

Logic-based hydrogel degradation in response to environmental stimuli

After validating linker behavior on the molecular level, we sought to characterize the logic-based stimuli-responsiveness of bulk materials. Each crosslinker was reacted independently with Alexa568®-labeled PEG-tetraBCN to form seventeen different types of fluorescent hydrogels. For each type, responsiveness to all eight input combinations involving reducing agents, light, and enzyme were evaluated. Hydrogel degradation was quantified by measuring supernatant fluorescence at non-kinetically limited endpoints following treatment (Fig. 3, Supplementary Methods 27 and 28, Supplementary Figs. 10 and 11). Each of the YES-gated materials (E, R, and P) behaved as expected, degrading only when the programmed cue was present. The high selectivity (>10-fold over non-specific release) again demonstrates the orthogonality of the employed stimuli-labile chemistries. The OR-gated materials (RVE, EVP, RVP) also responded as expected, degrading fully when either of the relevant cues was present. The AND-gated materials (RAE, EAP, RAP) also functioned properly, fully degrading only when both programmed cues were present. The observed release selectivity (>7-fold) is as or more specific than the most successful dual-input degradable materials previously reported^{12,14–16}. Of the three-input materials containing two logic gates, six of eight [i.e., EV(RAP), PV(RAE), RΛ(EVP), PΛ(RVE), RVEVP, RV(EAP)] behaved fully as designed, degrading with high selectivity only when the respective cues were present. The conditions $[E\Lambda(RVP)]_{EP}$ and $(R\Lambda E\Lambda P)_{REP}$ did not fully degrade, which we attribute to known decreased proteolytic cleavage kinetics for strained MMP-degradable substrates³⁴, in this case due to internal ring strain. These higher-order, three-input crosslinkers are the most complex logical operators ever used to control material degradation. This generalizable approach proves robust as 132 of the 136 treatment conditions yielded engineered degradation (defined as either complete degradation or <30% nonspecific release). The exhaustive synthesis and testing of each possible material demonstrates that complex biomaterial computation can be achieved with high fidelity through the hierarchical combination of simple YES/OR/AND logic gates. Given the initial success of this modular framework, we expect to be able to substitute the chosen stimuli-labile groups with any number of other chemically orthogonal moieties sensitive to pH, additional proteases, visible light, temperature, or ultrasound.

Disease-associated delivery of doxorubicin to an *in vitro* cancer model

To demonstrate the ability to deliver functional therapeutics in response to precise combinations of pathophysiological stimuli, we tethered a BCN-tagged doxorubicin (DOX) chemotherapeutic into RAE gels that degrade with high specificity to cancer microenvironmental cues (Fig. 4a–b, Supplementary Methods 29). Extent of hydrogel functionalization was chosen such that solution DOX concentration following full material degradation (44 μM) would yield population-wide apoptotic death of plated cervical cancer-derived HeLa cells (Fig. 4c). Following treatment by each relevant input combination (i.e., N, E, R, RE), cells were incubated in hydrogel supernatants for 48 hours prior to quantitative analysis of double-stranded DNA (dsDNA) content, indicative of the total number of viable cells. In the absence of treatment, or that with just reductant or MMP, normal proliferation was observed ($95 \pm 3\%$, $97 \pm 2\%$, and $76 \pm 5\%$, respectively, relative to non-treated controls lacking gels). The slight decrease in total dsDNA content following enzymatic treatment is attributed to secondary effects of the MMP treatment, rather than to non-specific DOX

release (Supplementary Method 29). In stark contrast to treatments with a single input, treatment with both inputs resulted in complete cell eradication ($1.8 \pm 0.2\%$ dsDNA content relative to controls), as designed. These results highlight the unique capacity of this approach to control release of functional small molecule therapeutics through logic-based gel degradation, enabling precise regulation of cell fate in response to disease-defined combinations of external cues.

Logic-based delivery of live cells from stimuli-responsive hydrogels

To illustrate the biocomputational response of these engineered materials to a combination of spatially defined as well as environmental cues, we formulated a multifunctional hydrogel comprised of three distinct logical regions (RAP, P, RVP), each labeled with a different fluorophore (Fig. 5). These hydrogels were sequentially exposed to masked UV light and reducing conditions, and imaged *via* fluorescent confocal microscopy (Supplementary Method 30). Each region responded to external cues as engineered, degrading only when the proper set of input conditions had been presented. To demonstrate cytocompatible gelation and multi-stimuli-responsive degradation, an analogous experiment was performed with each region containing encapsulated hS5 bone marrow-derived stromal cells that constitutively express a different fluorescent protein. Cells were released from gels following sequential masked light exposure, reducing conditions, and flood illumination, harvested after each treatment, and analyzed by flow cytometry. Each treatment yielded a distinct cell collection matching the expected color composition (Supplementary Method 31). Encapsulated cells were also shown to be viable when released through each stimulus, demonstrating whole process cytocompatibility (Supplementary Fig. 12). This material system, which yields sequential and environmentally triggered release of multiple cell lines in well-defined combinations, represents the most advanced live-cell delivery platform to date.

Discussion

Although we have first implemented our logic-gated approach to control biomaterial degradation using SPAAC-based PEG hydrogels that respond to reductant, enzyme, and light inputs, these general methodologies should be readily extendable to different stimuli-labile moieties, polymer compositions, and gelation chemistries. We hypothesize that these logic-based strategies can be extended to covalently tether other small molecules, peptides, proteins, polysaccharides, and nucleic acids to a non-degradable hydrogel *via* a stimuli-responsive linker, affording precise biochemical presentation through environmentally triggered controlled release of bioactive species.

Another potential benefit of our approach stems from the ability to tailor the “propagation delay” – the time required to transduce input signals into the appropriate functional output – of the Boolean operator for different therapeutic applications. For these logic-based materials, gate delay is governed by the susceptibility of each labile region to its relevant input, overall construct size/geometry, and the concentrations of the environmental cues triggering degradation. The degradation rate of a linkage to a given input may be tuned over several orders of magnitude, for example by modifying substituents on photodegradable

groups or substituting single amino acids within enzyme-labile peptide sequences^{24,35–37}. The propagation delay can be further decreased by formulating materials into geometries where response is reaction-limited rather than diffusion-limited. Careful choice of construct geometry and stimuli-labile group identity enables user-specified control over material response rates.

Capitalizing on this platform's unique capacity to govern material properties in response to combinations of both exogenous user-specified spatiotemporal cues (e.g., light) and endogenous cell-produced signals (e.g., enzymes, reductants) may enable new advances in 3D cell culture and tissue engineering. In one envisioned application, user-specified material photodegradation can be performed within EVP gels to generate customizable vasculature³⁸ within a synthetic environment that supports enzyme-mediated matrix remodeling and long-term cell survival. In another, cells encapsulated within a photopatterned EAP material will only undergo cell-mediated spreading within user-defined gel regions; we anticipate that such combined user and cellular control over the culture microenvironment will provide unique opportunities towards directing 4D stem cell differentiation^{29,39,40}.

Here we have introduced the first modular approach to engineer materials with tailored, user-specified, logic-based responsiveness to environmental cues. By controlling the molecular architecture and connectivity of multiple stimuli-labile moieties within discrete peptide-based crosslinkers, we have endowed biomaterials with unprecedented computational capacity through hierarchical combinations of Boolean YES/OR/AND gates. Having exhaustively synthesized crosslinkers that are each uniquely sensitive to combinations of three orthogonal inputs (i.e., enzyme, reduction, light), we have shown that constructs exhibit expected behavior spanning molecular and macroscopic scales. We have utilized these platforms to demonstrate the first sequential and spatiotemporally varied delivery of multiple cell lines from a single gel, as well as the controlled release of a functional chemotherapeutic in response to disease-associated cues. We expect that these platforms will find great utility in targeted drug delivery, where release of therapeutics, proteins, and cells can be confined to sites of disease with high selectivity, as well for applications in diagnostics, tissue engineering, and regenerative medicine.

Methods

Synthesis and characterization of logical crosslinkers

For complete details of all logical crosslinker syntheses and characterization, see Supplementary Methods 1–21. Briefly, peptides were generated by standard microwave-assisted Fmoc solid-phase peptide synthesis (CEM Liberty 1) and purified using reversed-phase high-pressure liquid chromatography (RP-HPLC, Dionex Ultimate 3000, C18 column). Peptide-based crosslinkers were characterized *via* MALDI-TOF mass spectrometry (Bruker AutoFlex II).

Assessing solution-based crosslinker degradation in response to external stimuli

Each crosslinker species (40 nmol) was dissolved in MMP buffer (110 μL , 200 mM sodium chloride, 50 mM tris, 5 mM calcium chloride, 1 μM zinc chloride, pH adjusted to 7.5 with hydrochloric acid) and exposed to each unique combination of enzyme, reductive, and light.

Samples receiving the reductive input (R) were treated with tris(2-carboxyethyl)phosphine hydrochloride (TCEP-HCl, 200 nmol) and all samples were incubated overnight (37 $^{\circ}\text{C}$). To quench any unreached TCEP, these samples were further treated with hydroxyethyl disulfide (HEDS, 500 nmol) and incubated (4 hr, 37 $^{\circ}\text{C}$). Samples receiving the enzyme input (E) were then treated with MMP-8 (5 μL , 0.2 mg mL^{-1} in MMP buffer) and all samples were incubated overnight (37 $^{\circ}\text{C}$). Samples receiving the light input (P) were subsequently exposed to UV light ($\lambda = 365$ nm, 10 mW cm^{-2} incident light, 60 minutes). All samples were diluted with acetonitrile/water (80:20, 100 μL) containing trifluoroacetic acid (0.1%) and characterized by MALDI-TOF; mass-to-charge ratios (m/z) of treated species were compared to expected products (Supplementary Figs. 1–9). Complete experimental detail is provided in Supplementary Method 24.

In situ rheology of hydrogel formation

Oscillatory rheological analysis (Anton Paar MCR301) was performed with a cone and plate geometry (25 mm diameter, 1 $^{\circ}$ cone) at 25 $^{\circ}\text{C}$ and 25 Hz with a 1% strain (conditions identified to be in the viscoelastic region). The EAP crosslinker was pre-treated with each combination of MMP (E) and/or light (P), as described above. A hydrogel precursor solution of PEG-tetraBCN (2 mM) and pre-treated EAP crosslinker (4 mM) in MMP buffer was reacted *in situ*, G' and G'' were monitored for 120 minutes. Complete experimental detail is provided in Supplementary Method 25.

Logic-based hydrogel degradation in response to sequential stimuli

Fluorescent hydrogels (10 μL) were formulated in microcentrifuge tubes from a precursor solution of PEG-tetraBCN-AF568 (2 mM) and a logical peptide crosslinker (4 mM) in MMP buffer (reacted 60 minutes, 25 $^{\circ}\text{C}$). Hydrogels were washed in MMP buffer. Every logical material was treated with each unique input combination in experimental triplicate, as described above. The extent of gel degradation was assessed through supernatant fluorescence quantification (SpectraMax M5, excitation: 570 nm, emission: 610 nm, emission cut-off filter: 590 nm). Complete experimental detail is provided in Supplementary Method 27.

In vitro cellular response to environmentally triggered degradation of a doxorubicin-hydrogel

Hydrogels (15 μL) were formulated with DOX (1 mM) from a precursor solution of PEG-tetraBCN (2 mM) and the RAE-DOX linker (4 mM, Supplementary Method 29) in a 4-(2-hydroxyethyl)-1-piperazineethanesulfonic acid (HEPES) buffer (5 mM HEPES, 3 mM CaCl_2 , 5 μM ZnCl_2). Gels were washed with HEPES buffer and treated with each set of relevant inputs in experimental triplicate. Hydrogel supernatant was collected and diluted (1:1) with 2x Dulbecco's Modified Eagle's medium. HeLa cells were cultured in this mixture (170 μL) in a 96-well plate for 48 hours (beginning 24 hours after HeLa seeding at 2

$\times 10^3$ cells well⁻¹), upon which cellular double-stranded DNA content was quantified with a PicoGreen® Assay (ThermoFisher). Complete experimental detail is provided in Supplementary Method 29.

Multi-logic hydrogel treatment and visualization

Hydrogels (130 μm thickness) were formulated with three distinct logically degradable regions, each labeled with a unique fluorophore: (i) R \wedge P crosslinker with AF568, (ii) P crosslinker with FAM, and (iii) RVP crosslinker with Cyanine5.

Hydrogels were imaged *via* fluorescent confocal microscopy. Preformed tri-color gels were exposed to UV light ($\lambda = 365$ nm, 10 mW cm⁻² incident light, 10 minutes) through a slitted photomask (alternating 200 μm wide lines and spaces) and imaged. Gels were subsequently treated with 2-mercaptoethanol [BME, 0.25 mM in 50 mL phosphate-buffered saline (PBS), 45 minutes, 25 °C] and imaged. Complete experimental detail is provided in Supplementary Method 30.

Hydrogel-encapsulated cell release studies

Hydrogels (130 μm thickness) were formulated with three distinct logically degradable regions, each encapsulating an hS5 cell line (40×10^6 cells mL⁻¹) that stably expresses a unique fluorescent protein: (i) R \wedge P crosslinker with hS5-mCherry⁺, (ii) P crosslinker with hS5-GFP⁺, and (iii) RVP crosslinker with hS5-BFP⁺. Cell-laden hydrogels were incubated overnight in media (RPMI-1640, 10% fetal bovine serum, 1% Penicillin-Streptomycin). Hydrogels were treated sequentially with light and reducing conditions, and imaged as described above.

Following each degradative step, released cells were collected and fixed (4% formaldehyde). Flow cytometry was performed on released cell populations (BD Biosciences LSR II Flow Cytometer). Forward scattering, side scattering, and the fluorescence corresponding to each protein were recorded for each event. Complete experimental and analytical details are provided in Supplementary Method 31.

Cell viability following hydrogel encapsulation and triggered release

hS5 cells (40×10^6 cells mL⁻¹) were encapsulated within each single-input responsive hydrogel (130 μm thick, either R, E, or P) in experimental triplicate, and stored in media for one hour. To induce gel degradation, R gels were treated with BME (0.25 mM in PBS, 37 °C, 45 minutes); P gels were exposed to UV light ($\lambda = 365$ nm, 10 mW cm⁻², 10 minutes); E gels were treated with MMP-8 (0.20 nM in RPMI, 37 °C, 60 minutes). Cells were collected, stained with a Live/Dead® assay (Invitrogen), and imaged (Nikon Eclipse TE2000-U). Cell viability was determined by standard image analysis. Complete experimental detail is provided in Supplementary Fig. 12.

Supplementary Material

Refer to Web version on PubMed Central for supplementary material.

Acknowledgments

The authors thank B. Hayes and B. Torok-Storb for gifting the hS5 cells, S. Adelmund for synthesizing and supplying BCN-OSu, E. Ruskowitz for useful discussion involving the DOX studies, as well as to Profs. K. Anseth, D. Tirrell, S. Pun, and B. Ratner for their constructive comments during the preparation of this manuscript. We gratefully acknowledge support from S. Edgar at the UW Mass Spectrometry Center, D. Prunkard at the UW Pathology Flow Cytometry Core Facility, and N. Peters and support from the NIH to the UW W. M. Keck Microscopy Center (S10 OD016240). This work was supported by a University of Washington Faculty Startup Grant (C.A.D.) and a National Science Foundation CAREER Award (DMR 1652141, C.A.D.).

References

1. Burdick JA, Murphy WL. Moving from static to dynamic complexity in hydrogel design. *Nat Commun.* 2012; 3:1269. [PubMed: 23232399]
2. Hoffman AS. Stimuli-responsive polymers: Biomedical applications and challenges for clinical translation. *Adv Drug Deliv Rev.* 2013; 65:10–16. [PubMed: 23246762]
3. Knipe JM, Peppas NA. Multi-responsive hydrogels for drug delivery and tissue engineering applications. *Regen Biomater.* 2014; 1:57–65. [PubMed: 26816625]
4. Mura S, Nicolas J, Couvreur P. Stimuli-responsive nanocarriers for drug delivery. *Nat Mater.* 2013; 12:991–1003. [PubMed: 24150417]
5. O'Neill HS, et al. Biomaterial-enhanced cell and drug delivery: Lessons learned in the cardiac field and future perspectives. *Adv Mater.* 2016; 28:5648–5661. [PubMed: 26840955]
6. Tibbitt MW, Rodell CB, Burdick JA, Anseth KS. Progress in material design for biomedical applications. *Proc Natl Acad Sci.* 2015; 112:14444–14451. [PubMed: 26598696]
7. Evans AC, Thadani NN, Suh J. Biocomputing nanoplatfoms as therapeutics and diagnostics. *J Control Release.* 2016; 240:387–393. [PubMed: 26826305]
8. Lu Y, Aimetti AA, Langer R, Gu Z. Bioresponsive materials. *Nat Rev Mater.* 2016; 2:16075.
9. DeForest CA, Anseth KS. Advances in bioactive hydrogels to probe and direct cell fate. *Annu Rev Chem Biomol Eng.* 2012; 3:421–444. [PubMed: 22524507]
10. Li J, Mooney DJ. Designing hydrogels for controlled drug delivery. *Nat Rev Mater.* 2016; 1:16071.
11. McCawley LJ, Matrisian LM. Matrix metalloproteinases: Multifunctional contributors to tumor progression. *Mol Med Today.* 2000; 6:149–156. [PubMed: 10740253]
12. Chen X, et al. Dual bioresponsive mesoporous silica nanocarrier as an 'AND' logic gate for targeted drug delivery cancer cells. *Adv Funct Mater.* 2014; 24:6999–7006.
13. Choh S, Cross D, Wang C. Facile synthesis and characterization of disulfide-cross-linked hyaluronic acid hydrogels for protein delivery and cell encapsulation. *Biomacromolecules.* 2011; 12:1126–1136. [PubMed: 21384907]
14. Douglas SM, Bachelet I, Church GM. A logic-gated nanorobot for targeted transport of molecular payloads. *Science.* 2012; 335:831–834. [PubMed: 22344439]
15. Ikeda M, et al. Installing logic-gate responses to a variety of biological substances in supramolecular hydrogel-enzyme hybrids. *Nat Chem.* 2014; 6:511–518. [PubMed: 24848237]
16. Komatsu H, et al. Supramolecular hydrogel exhibiting four basic logic gate functions to fine-tune substance release. *J Am Chem Soc.* 2009; 131:5580–5585. [PubMed: 19331364]
17. Liu G, Ji W, Feng C. Installing logic gates to multiresponsive supramolecular hydrogel co-assembled from phenylalanine amphiphile and bis(pyridinyl) derivative. *Langmuir.* 2015; 31:7122–7128. [PubMed: 26061452]
18. Motornov M, et al. 'Chemical transformers' from nanoparticle ensembles operated with logic. *Nano Lett.* 2008; 8:2993–2997. [PubMed: 18700803]
19. Kharkar PM, Kiick KL, Kloxin AM. Design of thiol- and light-sensitive degradable hydrogels using Michael-type addition reactions. *Polym Chem.* 2015; 6:5565–5574. [PubMed: 26284125]
20. de Garcia Lux C, et al. Short soluble coumarin crosslinkers for light-controlled release of cells and proteins from hydrogels. *Biomacromolecules.* 2015; 16:3286–3296. [PubMed: 26349005]
21. Roche ET, et al. Comparison of biomaterial delivery vehicles for improving acute retention of stem cells in the infarcted heart. *Biomaterials.* 2014; 35:6850–6858. [PubMed: 24862441]

22. Steinhilber D, et al. A microgel construction kit for bioorthogonal encapsulation and pH-controlled release of living cells. *Angew Chemie Int Ed*. 2013; 52:13538–13543.
23. Griffin DR, Kasko AM. Photodegradable macromers and hydrogels for live cell encapsulation and release. *J Am Chem Soc*. 2012; 134:13103–13107. [PubMed: 22765384]
24. Nagase H, Fields GB. Human matrix metalloproteinase specificity studies using collagen sequence-based synthetic peptides. *Pept Sci*. 1996; 40:399–416.
25. Kloxin AM, Tibbitt MW, Anseth KS. Synthesis of photodegradable hydrogels as dynamically tunable cell culture platforms. *Nat Protoc*. 2010; 5:1867–1887. [PubMed: 21127482]
26. Agard NJ, Prescher JA, Bertozzi CR. A strain-promoted [3 + 2] azide-alkyne cycloaddition for covalent modification of biomolecules in living systems. *J Am Chem Soc*. 2004; 126:15046–15047. [PubMed: 15547999]
27. DeForest CA, Anseth KS. Cytocompatible click-based hydrogels with dynamically tunable properties through orthogonal photoconjugation and photocleavage reactions. *Nat Chem*. 2011; 3:925–931. [PubMed: 22109271]
28. DeForest CA, Polizzotti BD, Anseth KS. Sequential click reactions for synthesizing and patterning three-dimensional cell microenvironments. *Nat Mater*. 2009; 8:659–664. [PubMed: 19543279]
29. DeForest CA, Tirrell DA. A photoreversible protein-patterning approach for guiding stem cell fate in three-dimensional gels. *Nat Mater*. 2015; 14:523–531. [PubMed: 25707020]
30. Madl CM, Katz LM, Heilshorn SC. Bio-orthogonally crosslinked, engineered protein hydrogels with tunable mechanics and biochemistry for cell encapsulation. *Adv Funct Mater*. 2016; 26:3612–3620. [PubMed: 27642274]
31. Jiang Y, Chen J, Deng C, Suuronen EJ, Zhong Z. Click hydrogels, microgels and nanogels: Emerging platforms for drug delivery and tissue engineering. *Biomaterials*. 2014; 35:4969–4985. [PubMed: 24674460]
32. Das RK, Gocheva V, Hammink R, Zouani OF, Rowan AE. Stress-stiffening-mediated stem-cell commitment switch in soft responsive hydrogels. *Nat Mater*. 2016; 15:318–25. [PubMed: 26618883]
33. Hiemenz, PC., Lodge, TP. *Polymer Chemistry*. CRC Press; 2007.
34. Flynn BP, et al. Mechanical strain stabilizes reconstituted collagen fibrils against enzymatic degradation by mammalian collagenase matrix metalloproteinase 8 (MMP-8). *PLoS One*. 2010; 5:e12337. [PubMed: 20808784]
35. Huo M, Yuan J, Wei Y. Redox-responsive polymers for drug delivery: From molecular design to applications. *Polym Chem*. 2014; 5:1519–1528.
36. Zhu C, Ninh C, Bettinger CJ. Photoreconfigurable polymers for biomedical applications: Chemistry and macromolecular engineering. *Biomacromolecules*. 2014; 15:3474–3494. [PubMed: 25226507]
37. Uhrich KE, Cannizzaro SM, Langer RS, Shakesheff KM. Polymeric systems for controlled drug release. *Chem Rev*. 1999; 99:3181–3198. [PubMed: 11749514]
38. Arakawa CK, Badeau BA, Zheng Y, DeForest CA. Multicellular vascularized engineered tissues through user-programmable biomaterial photodegradation. *Adv Mater*. 2017; 29:1703156.
39. Khetan S, Burdick JA. Patterning network structure to spatially control cellular remodeling and stem cell fate within 3-dimensional hydrogels. *Biomaterials*. 2010; 31:8228–8234. [PubMed: 20674004]
40. Khetan S, et al. Degradation-mediated cellular traction directs stem cell fate in covalently crosslinked three-dimensional hydrogels. *Nat Mater*. 2013; 12:458–65. [PubMed: 23524375]

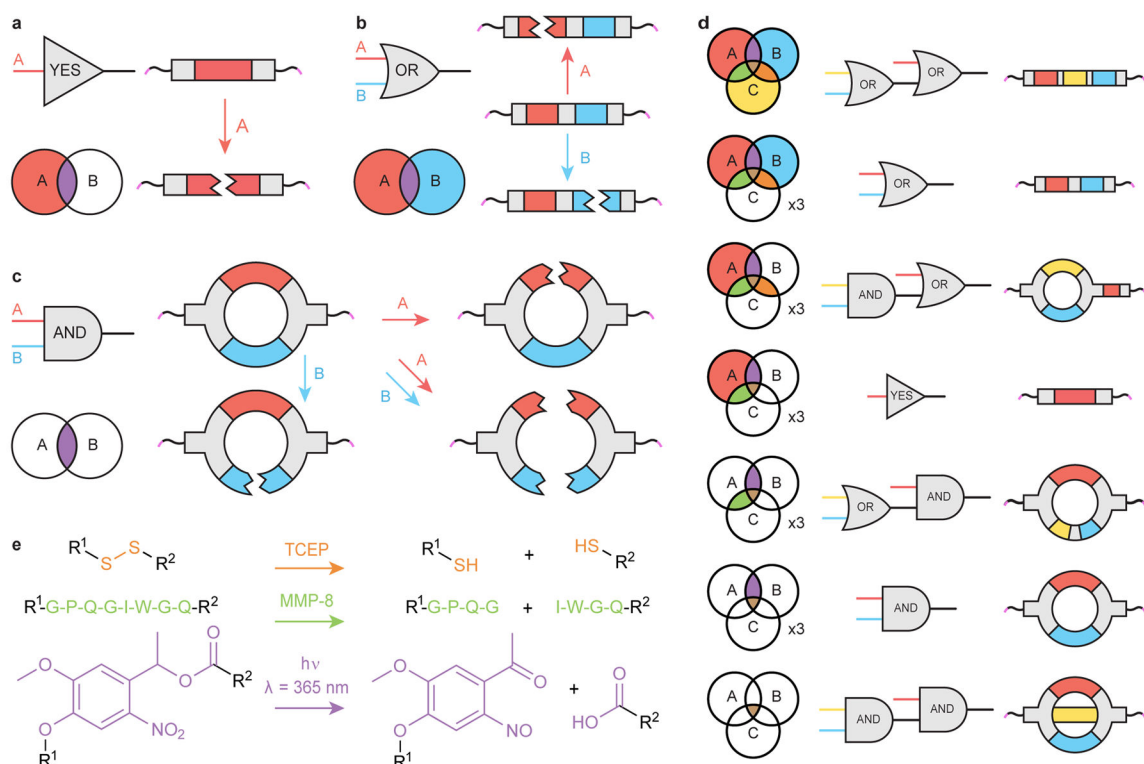


Figure 1. Rationally designed crosslinker architecture enables logic-based material degradation (a) The YES-gate material crosslinker contains a single stimuli-labile moiety (red). Presence of the corresponding chemical input cleaves this moiety, breaking covalent linkage between molecular endpoints (pink) to yield material degradation. Each region of the Venn diagram corresponds to a unique combination of inputs and indicates whether the material is expected to degrade (colored) or remain intact (white). (b) The OR-gate crosslinker contains two different stimuli-labile moieties (red and blue) connected in series. The presence of either relevant input cleaves the crosslinker, resulting in material degradation. (c) The AND-gate crosslinker contains two different stimuli-labile moieties (red and blue) connected in parallel. The presence of a single programmed input cleaves one linker arm but does not fully sever the crosslink, leaving material crosslinking density and mechanical properties unchanged. (d) Logic gates can be hierarchically combined to generate higher-order logical responses. Seventeen unique materials can be generated by combining three logic gates (YES, OR, AND) with three distinct inputs. (e) Reactions depicting cleavage of the stimuli-labile groups: disulfide bonds (orange) are reduced into free thiols, the proteolytically sensitive peptide sequence GPQG↓IWGQ (green) is enzymatically cleaved by MMP, and the *o*NB moiety (purple) undergoes photocleavage in the presence of near-UV light ($\lambda = 365$ nm).

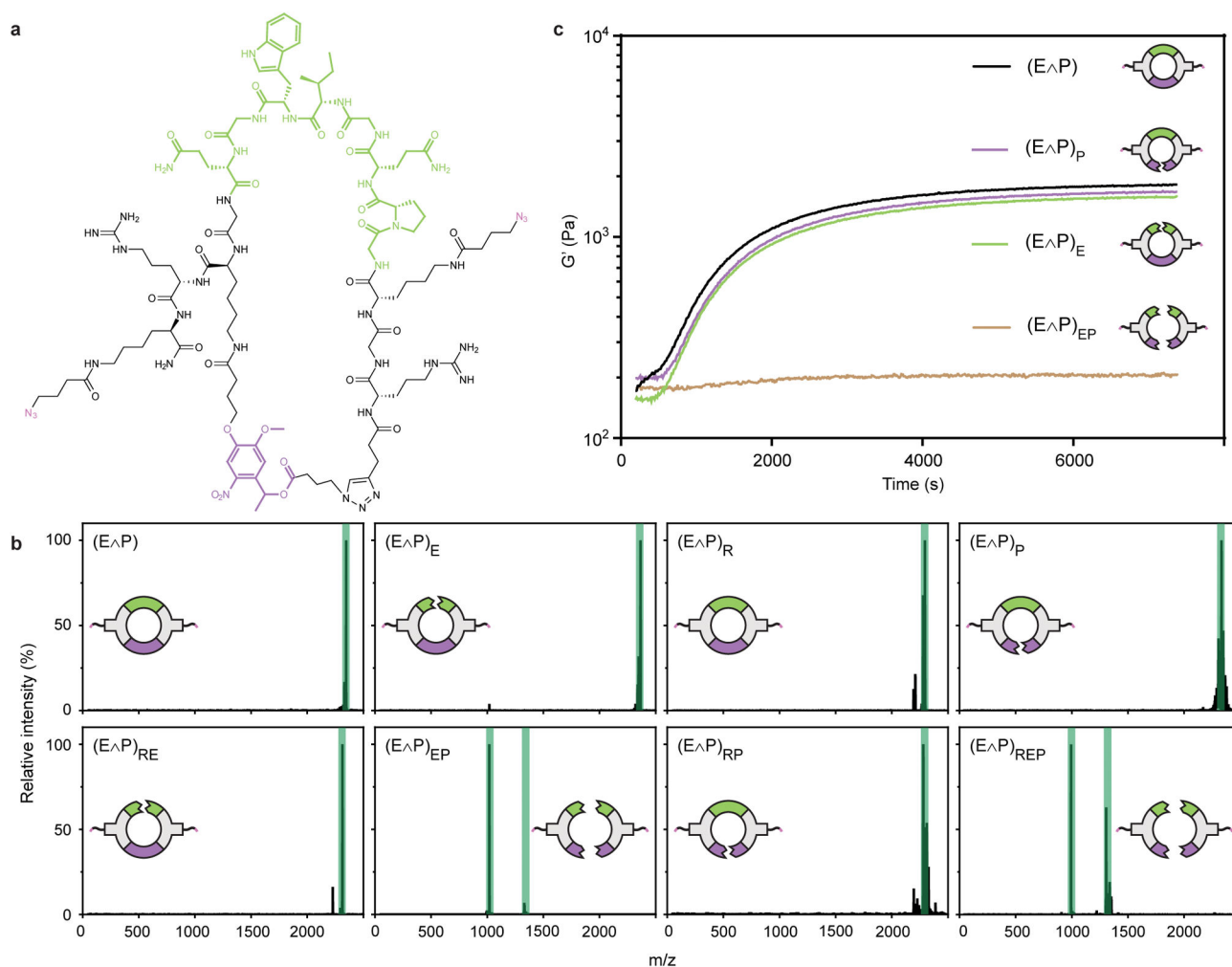


Figure 2. Engineered crosslinkers respond to environmental input combinations on the molecular level

(a) The chemical structure of the EAP crosslinker includes an MMP-degradable peptide sequence (green), a photolabile *o*NB moiety (purple), and two flanking azides (pink) for SPAAC-based hydrogel crosslinking. (b) The MALDI-TOF spectra of the EAP crosslinker after treatment with all unique combinations of enzyme (E), reductive species (R), and light (P) demonstrates correct molecular response followed each input combination. Expected product masses are highlighted in green. (c) *In situ* oscillatory rheological analysis of hydrogels crosslinked using treated EAP demonstrates that AND-gated materials require treatment by both relevant inputs to yield changes in bulk material properties.

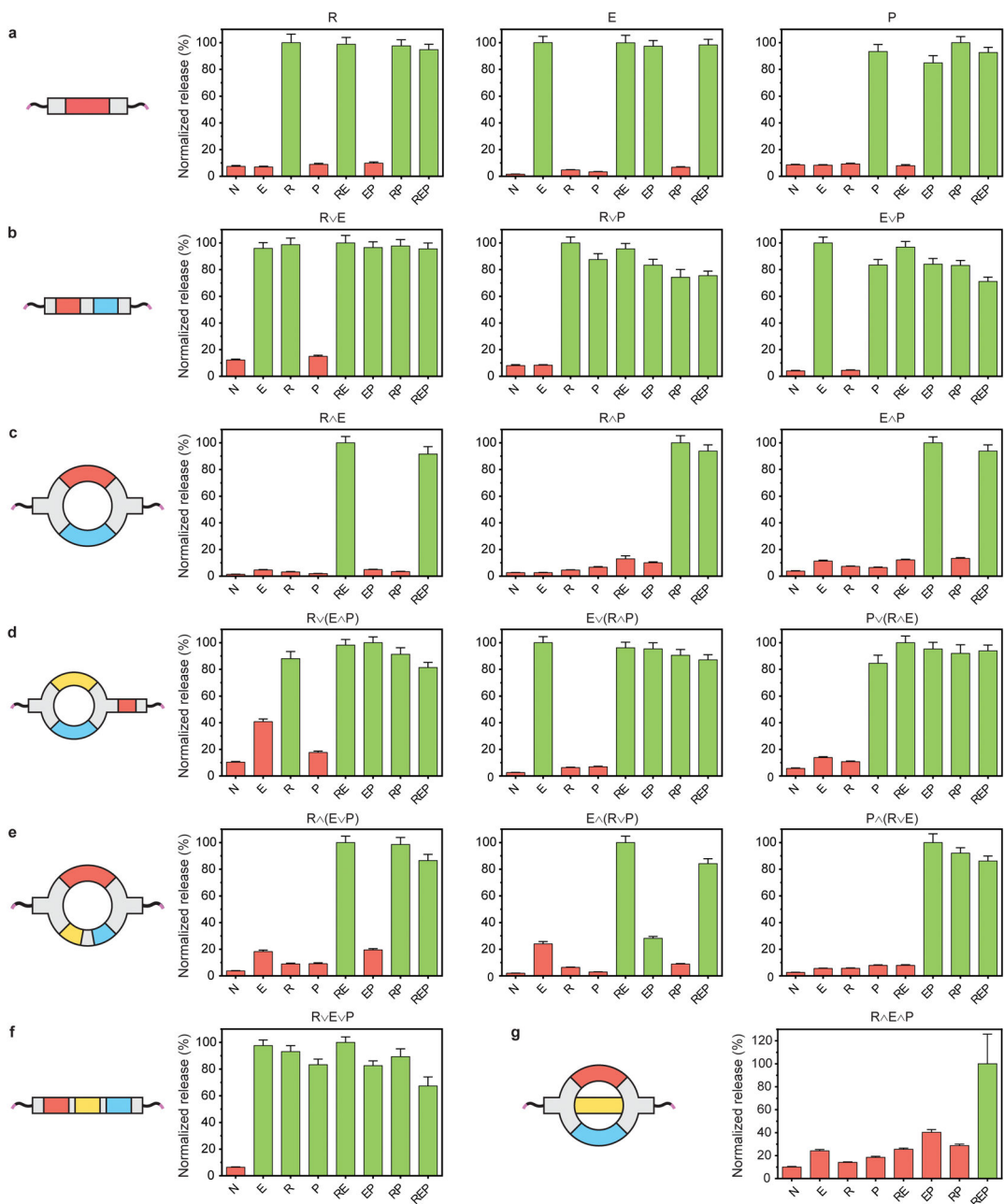


Figure 3. Logic-gated biomaterials exhibit programmable degradation in response to environmentally presented input combinations

(a) The response profiles of the single-input YES-gated materials. The response profiles of the two-input (b) OR-gated materials and (c) AND-gated materials. The response profiles of the higher-order, three-input (d) OR/(AND)-, (e) AND/(OR)-, (f) OR/OR-, and (g) AND/AND-gated materials. Plot titles correspond to crosslinker identity, with x-axis labels indicating material treatment conditions (N is no treatment, E is MMP enzyme, R is a chemical reductant, P is UV light). Green bars signify conditions expected to result in material degradation; red bars indicate conditions expected not to yield material degradation.

Error bars correspond to ± 1 standard deviation about the mean with propagated uncertainties for $n = 3$ experimental replicates.

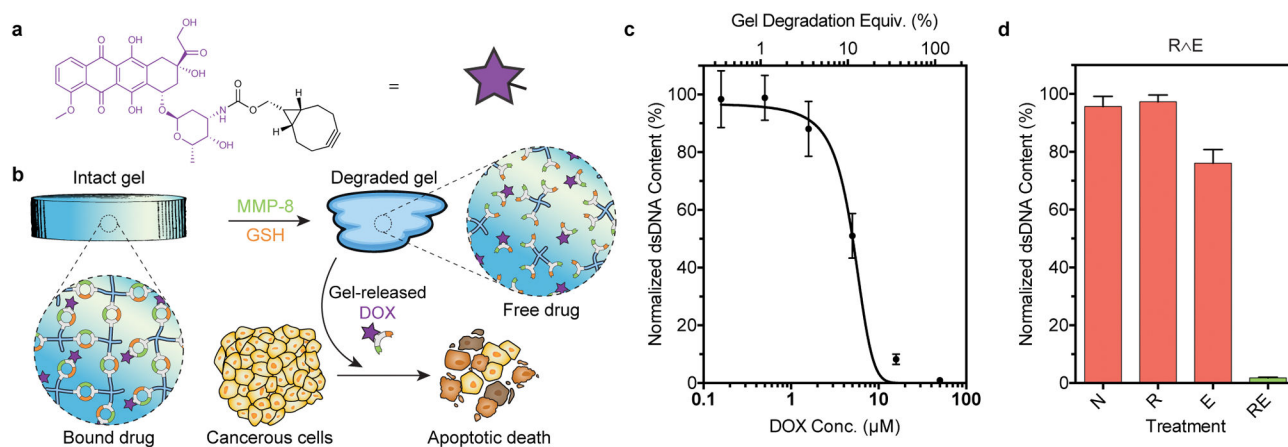


Figure 4. Logic-based doxorubicin delivery enhances specificity of HeLa cell death in presence of multiple disease-state hallmarks

(a) The chemical structure of doxorubicin functionalized at the amino group with BCN. (b) RAE hydrogel degradation is triggered in the presence of pathophysiological cues associated with tumor microenvironments: reducing conditions and MMPs. Liberated DOX induces apoptosis in cervical cancer-derived HeLa cells. (c) Dose-response curve of HeLa cells following treatment with RAE-DOX conjugate. (d) Normalized dsDNA content after culturing HeLa with released hydrogel components following varying treatments. X-axis label indicates material treatment conditions (N is no treatment, R is a chemical reductant, E is MMP enzyme). Green bars signify conditions expected to result in DOX release though material degradation; red bars indicate conditions expected not to yield material degradation. Error bars correspond to ± 1 standard deviation about the mean for $n = 3$ experimental replicates.

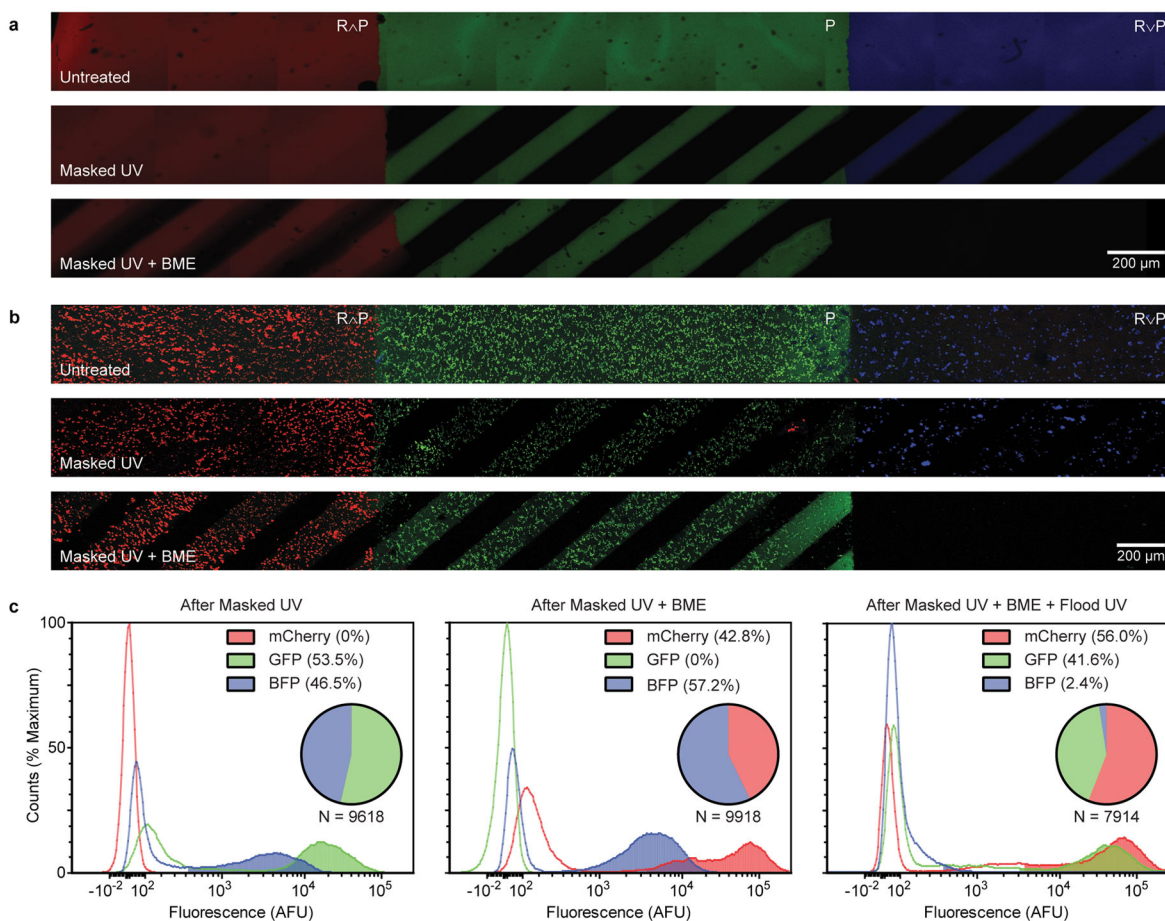


Figure 5. Sequential and spatiotemporally varied delivery of small molecules and cells from gels following logic-based response to environmental cues

(a) Spatially segregated regions of fluorescently labeled R (red), P (green), and V (blue) were formulated and imaged *via* confocal microscopy following sequential treatments of photomasked light and reducing conditions (β -mercaptoethanol, BME). Each region responded to the cues as engineered, degrading only in the presence of the proper set of input conditions. Scale bar, 200 μ m. (b) The experiment in panel A was repeated with encapsulated fluorescent cells [hS5 stably transfected to produce mCherry, Green Fluorescent Protein (GFP), and Blue Fluorescent Protein (BFP), respectively replacing the small molecule fluorophores]. Scale bar, 200 μ m. (c) The cells released from gels in panel B following sequential exposure to photomasked UV light, reducing conditions, and UV light flood exposure were quantified using flow cytometry. Histograms present fluorescence intensity for channels corresponding to each cell line with the shaded regions indicating positively gated cells.